Articles

Self-Assembly in Mixed Dialkyl Chain Cationic−Nonionic Surfactant Mixtures: Dihexadecyldimethyl Ammonium Bromide−Monododecyl Hexaethylene Glycol (Monododecyl Dodecaethylene Glycol) Mixtures

I. Tucker,[†] J. Penfold,*[,‡,§] R. K. Thomas,[§] I. Grillo,[∥] J. G. Barker,[⊥] and D. F. R. Mildner[⊥]

Unilever Research and Development Laboratory, Port Sunlight, Quarry Road East, Bebington, Wirral CH63 3JW, U.K., ISIS, STFC, Rutherford Appleton Laboratory, Chilton, Didcot, OXON, U.K., Physical and Theoretical Chemistry Laboratory, Oxford University, South Parks Road, Oxford, U.K., Institut Laue-Langevin, 6 Jules Horowitz, F-38042 Grenoble, Cedex 09, France, and National Institute of Standards and Technology, Center for Neutron Research, 100 Bureau Drive, Gaithersburg, Maryland 20899

The self-assembly of dialkyl chain cationic surfactant dihexadecyldimethyl ammonium bromide, DHDAB, and nonionic surfactants monododecyl hexaethylene glycol, $C_{12}E_6$, and monododecyl dodecaethylene glycol, $C_{12}E_{12}$, mixtures has been studied using predominantly small-angle neutron scattering, SANS. The scattering data have been used to produce a detailed phase diagram for the two surfactant mixtures and to quantify the microstructure in the different regions of the phase diagram. For cationic-surfactant-rich compositions, the microstructure is in the form of bilamellar, blv, or multilamellar, mlv, vesicles at low surfactant concentrations and is in an L_β lamellar phase at higher surfactant concentrations. For nonionic-rich compositions, the microstructure is predominantly in the form of relatively small globular mixed surfactant micelles, L_1. At intermediate compositions, there is an extensive mixed (blv/mlv) L_β/L_1 region. Although broadly similar, in detail there are significant differences in the phase behavior of DHDAB/$C_{12}E_6$ and DHDAB/$C_{12}E_{12}$ as a result of the increasing curvature associated with $C_{12}E_{12}$ aggregates compared to that of $C_{12}E_6$ aggregates. For the DHDAB/$C_{12}E_{12}$ mixture, the mixed (blv/mlv) L_β/L_1 phase region is more extensive. Furthermore, $C_{12}E_{12}$ has a greater impact upon the rigidity of the bilayer in the blv, mlv, and L_β regions than is the case for $C_{12}E_6$. The general features of the phase behavior are also reminiscent of that observed in phospholipid/surfactant mixtures and other related systems.

1. Introduction

Surfactant mixtures are commonplace in a wide range of consumer products such as detergents, shampoos, and conditioners. The mixing of different types of surfactants gives rise to synergies that provide the opportunity to optimize product performance. In such solutions, adsorption behavior, solution microstructure, and rheological properties can be manipulated to tailor the properties of the different products. As a result of their extensive applications and importance, surfactant mixing has been extensively studied, both theoretically and experimentally,[1,2] and many aspects are now relatively well understood. However, there remain many aspects that are poorly understood or relatively unexplored, especially in cases where extensive departures from ideal mixing are observed.

Dialkyl chain cationic surfactants are a major constituent of formulations such as hair and clothes care products and lubricants and are usually formulated with a range of other surfactants/cosurfactants, such as the polyoxethylene glycol nonionic surfactants.[3] Furthermore, there is a strong parallel with biomembranes, where the main ingredients are dialkyl chain lipids, and in membrane solubilization studies.[4] Although there is a relatively rich literature on the phase behavior of the dialkyl chain cationic surfactants,[5−9] there is relatively little on the phase behavior of the dialkyl chain cationic/nonionic surfactant mixtures and almost nothing on their associated surface adsorption behavior.[10,11] The dialkyl chain cationic surfactants will self-assemble into predominantly planar structures, lamellar or vesicular, which are structures that have low or zero spontaneous curvature. In contrast, the polyoxyethylene glycol nonionic surfactant (C_nE_m) aggregates can have a range of spontaneous

---

* Corresponding author. E-mail: j.penfold@rl.ac.ul.

† Unilever Research and Development Laboratory.
‡ ISIS.
§ Oxford University.
∥ Institut Laue-Langevin.
⊥ National Institute of Standards and Technology.

(1) Scamehorn J. F. In *Mixed Surfactant Systems*; Ogino, K., Abe, M., Eds.; Marcel Dekker: New York, 1997.
(2) Holland, P. M. Rubingh, D. N. In *Cationic Surfactants*; Holland, P. M.,. Rubingh, D. N.,. Eds.; Surfactant Science Series; Marcel Dekker: New York, 1990; *Vol. 37*
(3) Penfold, J.; Staples, E.; Ugazio, S.; Tucker, I.; Soubiram, L.; Hubbard, J.; Noro, M.; O'Malley, B.; Ferrante, A.; Ford, G.; Buron, H. *J. Phys. Chem. B* **2005**, *109*, 18107.

(4) Almgren, M. *Biochem Biophys Acta* **2000**, *1508*, 146.
(5) Dubois, M.; Zemb, T. *Langmuir* **1991**, *7*, 1357.
(6) Zemb, T.; Gazeau, D.; Dubois, D.; Gulik-Krnywicki, T. *Europhys. Lett.* **1993**, *21*, 759.
(7) Hass, S.; Hoffmann, H.; Thunig, C.; Hoinkis, I. E. *Colloid Polym. Sci.* **1999**, *277*, 856.
(8) Brady, J. E.; Evans, D. F.; Warr, G. G.; Grieser, F.; Ninham, B. W.; Ninham, B. W. *J. Phys. Chem.* **1986**, *90*, 1853.
(9) Caboi, F.; Moduzzi, M. *Langmuir* **1996**, *12*, 3548.
(10) Penfold, J.; Staples, E.; Tucker, I.; Thomas, R. K. *Langmuir* **2004**, *20*, 1269.
(11) Penfold, J.; Staples, E.; Tucker, I.; Soubiran, L.; Creeth, A.; Hubbard, J. *Phys. Chem. Chem. Phys.* **2000**, *2*, 5230.

curvatures, from planar to highly curved micellar structures, depending upon the ethylene oxide chain length and the alkyl to ethylene oxide chain length ratio, n/m.

The phase behavior of the individual dialkyl chain cationic surfactant, DHDAB, and the nonionic surfactants, $C_{12}E_6$ and $C_{12}E_{12}$, is well established. However, the evolution of the microstructure of mixtures of DHDAB with $C_{12}E_6$ and $C_{12}E_{12}$, components whose aggregates have very different preferred curvatures, has not been studied in any detail. In particular, how a predominantly planar structure evolves into one that is highly curved and the extent of any coexistence region have not been investigated or quantified in detail. An exception to this is the related work on the impact of surfactants (especially nonionic surfactants) on phospholipid membranes,[4] specifically, the effect of nonionic surfactant $C_{12}E_5$ on the phospholipid, DMPC, membranes.[12,13] Comparison with these studies and other related work is made in the Discussion.

In this article, we investigate the evolution of the solution microstructure (self-assembly) of the dialkyl chain cationic/nonionic surfactant mixtures of dihexadecyl dimethyl ammonium bromide, DHDAB, and monododecyl hexaethylene glycol, $C_{12}E_6$, and monododecyl dodecaethylene glycol, $C_{12}E_{12}$ These surfactants were selected on the basis of having broadly similar physical properties to those used commercially while also being readily available in both protonated and deuterated forms at high purity. Measurements are made over a range of compositions, from cationic- to nonionic-rich, and for a range of concentrations, from dilute to concentrated solutions. The impact of the cosurfactant, whose aggregates have an increasingly large curvature, is investigated by replacing $C_{12}E_6$ with $C_{12}E_{12}$. Although there is an asymmetry in the alkyl chain length between the cationic and nonionic surfactants, because the chain length of the nonionic is constant it is expected that the headgroup size change will be the significant factor. The measurements were made using predominantly small-angle neutron scattering, SANS, complementary optical texture measurements, some limited light scattering, PCS, ultra-small-angle scattering, USANS, and cryo-TEM measurements. Complementary measurements on the solution behavior of DHDAB and DHDAB/$C_{12}E_3$ mixtures (where both components are predominantly planar) are reported elsewhere.[14],[15] In the context of the range of applications of such mixtures, the adsorption behavior is crucially important, and the interplay between the adsorption behavior and the associated evolution in the solution microstructure is also reported separately.[16]

2. Experimental Details

i. Small-Angle Neutron Scattering, SANS. The SANS measurements were made in dilute solution (1.5 mM) on the D22 diffractometer at the ILL, France,[17] and measurements at higher surfactant concentrations (>10 mM) were made on the D11 diffractometer[17] and on the LOQ diffractometer at ISIS, U.K.[18] On D22, the measurements were made at a neutron wavelength, λ, of 8Å and a $\Delta\lambda/\lambda$ of 10% and two sample-to-detector distances, 3.5 and 16.5 m, to cover a scattering vector, Q, range of 0.002−0.2 Å^{-1}

(where the scattering vector, Q, is defined as $Q = 4\pi/\lambda \sin(\theta/2)$, and θ is the scattering angle). The D11 measurements were made at a neutron wavelength, λ, of 6 Å, and a $\Delta\lambda/\lambda$ of 10% and three sample-to-detector distances of 1.1, 5.0, and 16.5 m to cover a scattering vector, Q, range of 0.003−0.25 Å^{-1}. On LOQ, the measurements were made using the white beam time-of-flight method using neutron wavelengths in the range of 2−10 Å and a sample-to-detector distance of 4 m to cover a Q range of 0.008−0.25 Å^{-1}. All of the LOQ measurements were made with an 8 mm diameter beam and on D11 and D22 using a 7×10 mm beam. The data were corrected for background scattering, detector response, and spectral distribution of the incident beam (for LOQ) and converted to an absolute scattering cross section, $d\sigma/d\Omega$, (in cm^{-1}), using standard procedures.[19,20]

Some USANS measurements were made on a limited subset of samples using the Bonse−Hart double-crystal diffractometer, BT5, at NIST.[21] These measurements extended the accessible Q range to 5×10^{-5} Å^{-1} (measurements were made in the Q range of 5×10^{-5} to 5×10^{-3} Å^{-1}) to provide an estimate of the overall size of the predominantly cationic-rich planar structures (lamellar fragments, vesicles). The data were normalized and desmeared using standard procedures.[22]

ii. Other Experimental Techniques. Optical texture measurements were made using white unpolarized light and were used to provide an initial qualitative evaluation of the solution-phase behavior.

Dynamic light scattering measurements were made using a Malvern PCS8/4700 instrument and 7132A correlator. Data were collected in triplicate with run times of 120 s, and the individual autocorrelation functions obtained were analyzed using the Contin method to obtain the particle size distributions.[23] These measurements provided an additional and important independent estimate of the overall size of the cationic-rich microstructures (lamellar fragments, vesicles).

Some cryo-TEM measurements, using freeze−fracture replication,[24] were made to reinforce the interpretation of the cationic-rich lamellar structures.

iii. Materials and Measurements Made. The SANS measurements were made for the DHDAB/$C_{12}E_6$ and DHDAB/$C_{12}E_{12}$ mixtures at a concentration of 1.5 mM for solution compositions from pure DHDAB, 100:0, to pure nonionic, 0:100, at 10% intervals in composition (cationic/nonionic mole ratio). For DHDAB/$C_{12}E_6$ measurements were made at higher surfactant concentrations, in the range of 10−160 mM, over the entire composition range (at compositions of 100:0, 80:20, 40:60, 50:50, 60:40, and 30:70). For the DHDAB/$C_{12}E_{12}$ mixtures, a similar range of surfactant concentrations and compositions were measured, except that no measurements were made for solutions richer in nonionic surfactant than 40:60.

The DHDAB was obtained from Fluka and was recrystallized from ethyl acetate. $C_{12}E_6$ was obtained from Nikko Chemicals Japan and was used as supplied. $C_{12}E_{12}$ was custom synthesized by Unilever Research and Development, Port Sunlight,[25] and its purity was verified by NMR and surface tension measurements.

All of the SANS measurements were made for solutions in D$_2$O (Flurochem) in 1 mm path length Starna quartz spectrophotometer cells. The cells were cleaned in Decon 90 and rinsed in pure water (Elga Ultrapure). All of the samples were measured at 30 ± 1 °C, above the Krafft point of 28 °C for pure DHDAB.[14] The samples were prepared by heating to 60 °C to dissolve the materials and then cooling to and maintaining a temperature in excess of 30 °C. Under such conditions, at no stage in the sample preparation and storage

(12) Konig, S.; Meleard, P.; Navailles, L.; Roux, D.; Nuovo, Il. *Cimento* **1994**, *16*, 1585.

(13) Moreau, P.; Navailles, L.; Giermanska-Kahn, J.; Mondain-Monval, O.; Nallet, F.; Roux, D. *Europhys. Lett.* **2006**, *73*, 49.

(14) Tucker, I.; Penfold, J.; Thomas, R. K.; Grillo, I.; Barker, J.; Mildner, D. *Langmuir* **2008**, in press.

(15) Tucker, I.; Penfold, J.; Thomas, R. K.; Grillo, I. To be submitted for publication.

(16) Tucker, I.; Penfold, J.; Thomas, R. K. To be submitted for publication.

(17) *Neutron beam facilities at the high flux reactor available for users, ILL, Grenoble, France,* 1994.

(18) Heenan, R. K.; King, S. M.; Penfold, J. *Appl. Cryst.* **1997**, *30*, 1140.

(19) Ghosh, R. E.; Egelhaaf, S. U.; Rennie, A. R. *ILL Int. Rep.* **1998**, ILL98GH14T

(20) Heenan, R. K.; King, S. M.; Osborn, R.; Stanley, H. B. *RAL Int. Rep.* **1989**, RAL-89-128.

(21) Barker, J. G.; Glinka, C. J.; Moyer, J. J.; Kim, M. H.; Drews, A. R.; Agamalian, M. *J. Appl. Crystallogr.* **2005**, *38*, 1004–1011.

(22) Lake, J. A. *Acta Crystallogr.* **1967**, *23*, 191.

(23) Provencher, S. W. *Makromol. Chem.* **1979**, *180*, 201.

(24) (a) Danino, D.; Bernheim-Groswasser, A.; Talmon, Y. *Colloids Surf., A* **2001**, *183−185*, 113. (b) Talmon, Y. *Ber. Bunsen.-Ges. Phys. Chem.* **1996**, *100*, 364.

(25) Conroy, J.; Unilever R and D; private communication.

of the DHDAB/nonionic surfactant mixtures was there any indication of a significant change in the Krafft temperature. Measurement at 30 °C also minimizes any complications that would arise from approaching the cloud point of $C_{12}E_6$. Dilute solutions (up to 80 mM) were prepared by dispersion in D_2O at an elevated temperature to melt the surfactant and mild stirring to disperse the material. At higher concentrations (>80 mM), more vigorous mixing by extrusion and annealing at higher temperatures (80 °C) was required to ensure complete dissolution and mixing.

iv. SANS Data Analysis. The form of the SANS scattering patterns (Q dependence) was used qualitatively to identify the lamellar (vesicular), micellar, and mixed-phase regions of the overall phase behavior. In the purely lamellar (vesicular) and micellar regions, detailed quantitative analysis was also made using standard modeling procedures for mixed surfactant micelles[26] and for lamellar dispersions.[27]

The scattering from globular surfactant micelles in aqueous solution is described by the decoupling approximation, derived by Hayter and Penfold[26] such that

$$\frac{d\sigma}{d\Omega} = n[S(Q)|\langle F(Q)\rangle_Q|^2 + \langle|F(Q)|^2\rangle_Q - |\langle F(Q)\rangle_Q|^2] \quad (1)$$

where the averages denoted by $\langle Q\rangle$ are averages over particles size and orientation, n is the micelle number density, $S(Q)$ is the intermicellar structure factor, and $F(Q)$ is the micelle form factor. The micelle structure (form factor, $F(Q)$) is modeled using a standard core-and-shell model,[26] where the form factor for globular micelles is

$$F(Q) = V_1(\rho_1 - \rho_2) F_0(QR_1) + V_2(\rho_2 - \rho_s) F_0(QR_2) \quad (2)$$

and R1 and R2 are the core and shell radii, $V_i = 4\pi R_i^3/3$, $F_0(QR_i) = 3j_1(QR_i)/(QR) = 3[\sin(QR) - QR\cos(QR)]/(QR)^3$, ρ_1, ρ_2, and ρ_s are the scattering-length densities of the micelle core, shell, and solvent, and $j_1(QR_i)$ is a first-order spherical Bessel function. The decoupling approximation assumes that for interacting (finite $S(Q)$) globular micelles there is no correlation among position, size, and orientation. The structure factor, $S(Q)$, which quantifies the intermicellar interactions/correlations, is included using the rescaled mean spherical approximation, RMSA, calculation[28,29] for a repulsive screened Coulombic intermicellar interaction potential characterized by the surface charge of the micelle, z, the Debye−Huckel inverse screening length, κ_{dh}, (defined in the usual way), and the micelle number density, n. The form factor, $F(Q)$, described in detail elsewhere,[26] is for a core−shell model constrained to fill space with an inner core of alkyl chains with an inner radius of $R1 \leq l$ (fully extended alkyl chain length) and where the outer shell contains the headgroups and associated hydration. For aggregation numbers greater than that which will pack into a sphere of radius R,l the model incorporates elliptical growth with a minor radius of $R1$ and a major radius of $eR1$, and the form factor (eq 2) used is now that for an ellipse rather than a sphere.[30] For nonelliptical micellar structures, polydispersity, characterized by the width of a Schultz distribution, is included analytically.[30] For the dialkyl chain surfactants, an additional parameter, ext, is required. This allows the constraint on the inner radius ($R1 \leq l$) to be relaxed such that it can be less than or greater than Rl by the factor ext. It can be considered to be a packing parameters that allows the partial molar volume of the alkyl chains in the micelle core to be adjusted as a result of additional packing constraints introduced by the dichain component. In the mixed surfactant systems, the two surfactant components are accommodated by assuming ideal mixing. From the known molecular

volumes, dimensions, and scattering lengths for the different surfactant and surfactant components, the model can be calculated, with the aggregation number, ν, micelle surface charge, z, and ext as refinable parameters.

The approach developed by Nallet et al.[27] has been used to analyze quantitatively the lamellar/vesicle scattering. Analysis of the scattering pattern yields an estimate of the Caille parameter (which is related to lamellar membrane rigidity and determines the width of the lamellar Bragg peaks in the scattering), the number of layers/lamellae, the bilayer spacing, d, and the thickness of the bilayer, δ. An analytical expression for $d\sigma/d\Omega$ takes into account the lamellar form factor, $P(Q)$, and the structure factor, $S(Q)$, taking into account membrane fluctuations and the contribution of resolution to the line width and assuming a powder average such that

$$\frac{d\sigma}{d\Omega} = 2\pi \frac{V}{d}\frac{1}{Q^2}P(Q)\,\bar{S}(Q) \quad (3)$$

$$P(Q)\frac{4}{Q^2}\Delta\rho^2\sin^2\left(Q\frac{\delta}{2}\right) \quad (4)$$

$$\bar{S}(Q) = 1 + 2\sum_1^{N-1}\left(1 - \frac{n}{N}\right)\cos\left(\frac{Qdn}{1 + 2\Delta Q^2 d^2\alpha(n)}\right)e - $$
$$\frac{2Q^2 d^2\alpha(n) + \Delta Q^2 d^2 n^2}{2(1 + 2\Delta Q^2 d^2\alpha(n))}\frac{1}{\sqrt{1 + 2\Delta Q^2 d^2\alpha(n)}} \quad (5)$$

where for small n

$$\langle(u_n - u_0)^2\rangle = \frac{\eta n^2 d^2}{8} \quad (6)$$

and $\alpha(n)$ is the correlation function

$$\alpha(n) = \langle(u_n - u_0)^2\rangle/2d \quad (7)$$

N is the number of layers in a lamellar fragment, u_o is the displacement of the nth layer from its equilibrium position in the z direction, and η is the Caille parameter, which is related to the membrane rigidity such that

$$\eta = \frac{Q_0^2 k_B T}{8\pi\sqrt{KB}} \quad (8)$$

B and K are the bilayer compressibility and bending modulus of the bilayer assembly, ΔQ is the instrumental resolution, d is the lamellar d spacing, δ is the bilayer width, $d = \delta/\phi$ (where ϕ is the volume fraction), $Q_0 = 2\pi/d$, and K is related to the single bilayer bending modulus, κ, where $\kappa = K_d$.

3. Results

I. DHDAB/$C_{12}E_6$ Structure. A preliminary qualitative evaluation of the phase behavior of the DHDAB/$C_{12}E_6$ surfactant mixture was made by recording the variation in the optical texture of the solutions with concentration and composition, as shown in Figure 1.

The nonionic-rich solutions are clear, consistent with small globular micelles, whereas the cationic-rich solutions exhibit a strong hue and a transition to greater turbidity at higher surfactant concentrations, consistent with larger aggregate structures such as lamellar vesicles. At intermediate compositions, there is a transition in the optical appearance between those two extremes. Although these observations provide an important initial qualitative evaluation and demonstrate the evolution of a predominantly micellar to lamellar structure, the fine detail of those structures and the extent of the region of coexistence are not quantifiable from such data.

SANS has been used primarily to obtain more detailed information about the composition and concentration dependence of the phase behavior and microstructure and to provide a more

(26) Hayter, J. B.; Penfold, J. *Colloid Polym. Sci.* **1983**, *261*, 1072.
(27) Nallet, F.; Laversanne, R.; Roux, D. *J. Phys. II* **1995**, *3*, 487.
(28) Hayter, J. B. In *Proceedings of Enrico Fermi School of Physics*; Varenna, Italy, 1983..
(29) Hayter, J. B.; Penfold, J. *Mol. Phys.* **1981**, *42*, 109.
(30) Hayter, J. B.; Hansen, J. P. *Mol. Phys.* **1982**, *42*, 651.
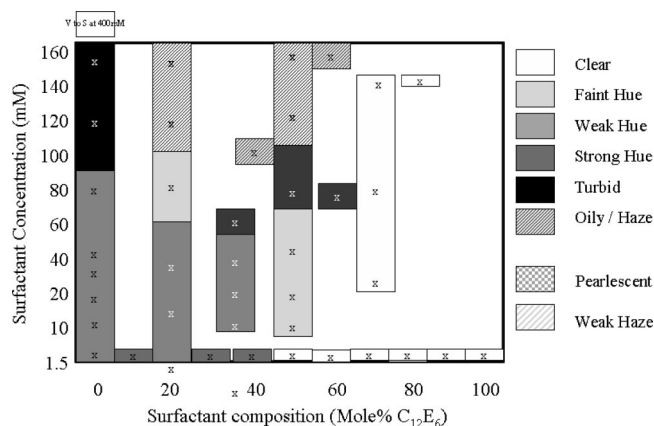
Figure 1. Variation in optical texture with surfactant concentration (mM) and composition (mole % $C_{12}E_6$) for DHDAB/$C_{12}E_6$ mixtures at 30 °C (each x denotes a point where the measurements were made), and the index for the different regions is included.

detailed quantified evaluation of those structures. Figure 2a shows the SANS data for the DHDAB/$C_{12}E_6$ mixture at a concentration of 1.5 mM in the composition range of 100:0−0:100.

Over the entire composition range, the 2-D scattering patterns are isotropic such that at this concentration there are no effects due to preferred orientations in the systems studied. For the cationic-rich compositions, the scattering has a Q^{-2} dependence (for $Q \leq 0.05$ Å^{-1}), consistent with planar structures, with well-defined oscillations (with a relatively large spacing, ∼1000 Å) originating from the lamellar structure. For nonionic-rich compositions, the scattering is consistent with that arising from globular micelles. As the cationic/nonionic composition increases from 0:100 to 30:70, the micelle scattering reflects the increasing charge on the micelles, and the formation of a peak, due to the intermicellar structure factor $S(Q)$, occurs. The scattering is also consistent with smaller micelles as the cationic content increases. The increasing charge results in a larger headgroup repulsion, a larger effective area/molecule, and hence smaller micelles. Between the surfactant compositions of 40:60 and 80:20 to 70:30, the scattering is consistent with the coexistence of planar/lamellar structures and globular micelles. This is seen more clearly in Figure 2b, where the scattering intensity is plotted in the form of $Q^2I(Q)$ versus Q. Here the transition from a Q^{-2} dependence to the mixed micellar/lamellar region and to the region consisting of globular micelles is more clearly illustrated. For compositions in the range of 100:0−80:20, the data have been quantitatively analyzed using the Nallet model (eqs 3−5) for a bilamellar vesicle structure with a bilayer thickness of $\delta \approx 35$ Å, a bilayer spacing of ∼1000 Å, and a relatively small Caille parameter of $\eta \approx 0.1$. Typical model fits are shown in Figure 3a, and the key model parameters are summarized in Table 1. A schematic representation of the bilamellar structure is shown in ref 14.

At a concentration of 1.5 mM and in the composition range of 100:0−70:30, the bilayer spacing is relatively large and increases as the cationic surfactant is diluted with nonionic surfactant. The small value of the Caille parameter ($\eta \approx 0.1$) is consistent with a relatively rigid membrane. The bilayer (or membrane) thickness increases with the addition of the nonionic surfactant. The periodicity of the oscillations is not consistent with that arising from unilamellar vesicles, where the fringe spacing would in that case reflect the overall size of the vesicle. The detailed Nallet analysis (parameters in Table 1) is consistent with a bilayer structure ($N = 2$). Attempts to model this data with $N > 2$ (as required for multilamellar vesicles or lamellar fragments) results in less satisfactory fits to the data, as more

pronounced Bragg oscillations arise. Included also in Figure 3a is the best model fit to the 100:0 data for a core + shell unilamellar vesicle model from ref 14, and this illustrates well the shortcomings of that model.

In the purely micellar region (compositions of 0:100−30:70), the scattering data have been analyzed using an established model for interacting globular micelles (eqs 1 and 2), as described in detail by Hayter and Penfold.[26] Typical model fits are shown in Figure 3b, and the key model parameters are summarized in Table 1. The parameters in Table 1 (and the associated model fits) show that for compositions in the range of 30:70−10:90 the micelles increase in size from relatively globular micelles with an aggregation number of ∼150 at 30:70 to a structure consistent with more elongated micelles at 10:90, with an aggregation number of ∼450. The data for pure $C_{12}E_6$ at 1.5 mM is consistent with highly elongated wormlike micelles. Here, the Hayter−Penfold model is no longer applicable, and a quantitative analysis of that data has not been made. A closer inspection of the scattering data in the mixed micellar/lamellar region for compositions mole ratios of DHDAB/$C_{12}E_6$ in the range of 40:60−70:30 shows that for compositions from 40:60−60:40 the data are consistent with the coexistence of micelles and lamellae, where the micellar contribution is dominant, as denoted by the L_1/L_β coexistence. At a DHDAB/$C_{12}E_6$ composition of 70:30, the data are consistent with the coexistence of lamellae (either L_β or mlv) and micelles, where the lamellar component is dominant, as denoted by L_β (mlv)/L_1.

SANS measurements were also made at higher surfactant concentrations in the concentration range of 10−160 mM. Here, the measurements were made predominantly in the lamellar and mixed lamellar/micellar regions, extending from pure DHDAB up to a nonionic-rich composition of 30:70. This was sufficient to establish the boundary between the mixed lamellar /micellar and micellar regions of the phase behavior. The data at the higher surfactant concentrations, although broadly similar to that measured at 1.5 mM, reflect the richer pattern of structures that exist in the evolution from blv (at 1.5 mM) to mlv or an L_β phase at higher surfactant concentrations. In Figure 4, the data for a composition of 80:20 and for concentrations from 20 to 160 mM are plotted. The increasing visibility of the Bragg oscillations in the data (in the region of $Q = 0.03$ Å^{-1}) is now consistent with the formation of mlv or an L_β phase. In the composition range of 40:60−60:40, the data are consistent with L_β/L_1 coexistence over the concentration range measured. Between 80 and 100 mM in this mixed region, there is a marked change in the form of the data, and this is ascribed to a change in the relative amounts of L_β and L_1, as indicated at a composition of 50:50 in Figure 4b.

Table 2 summarizes the key model parameters from the data at solution compositions of 80:20 and 65:35 (where single phase), which have been quantitatively analyzed using the Nallet model,[27] as described earlier.

ii. DHDAB/$C_{12}E_{12}$ Structure. Measurements of similar scope and range to those made for DHDAB/$C_{12}E_6$ were also made for DHDAB/$C_{12}E_{12}$. The optical texture observations were broadly similar to those made for DHDAB/$C_{12}E_6$ and are shown in Figure 5.

A notable difference is that the clear (micellar) region extends to solutions richer in DHDAB, and the region of weak/faint hue, attributed to mixed-phase behavior, is more extensive.

The SANS data for DHDAB/$C_{12}E_{12}$ in both dilute and concentrated solutions are broadly similar to those measured for DHDAB/$C_{12}E_6$ but also show in detail some rather distinct differences. Figure 6 shows the SANS data for 1.5 mM DHDAB/
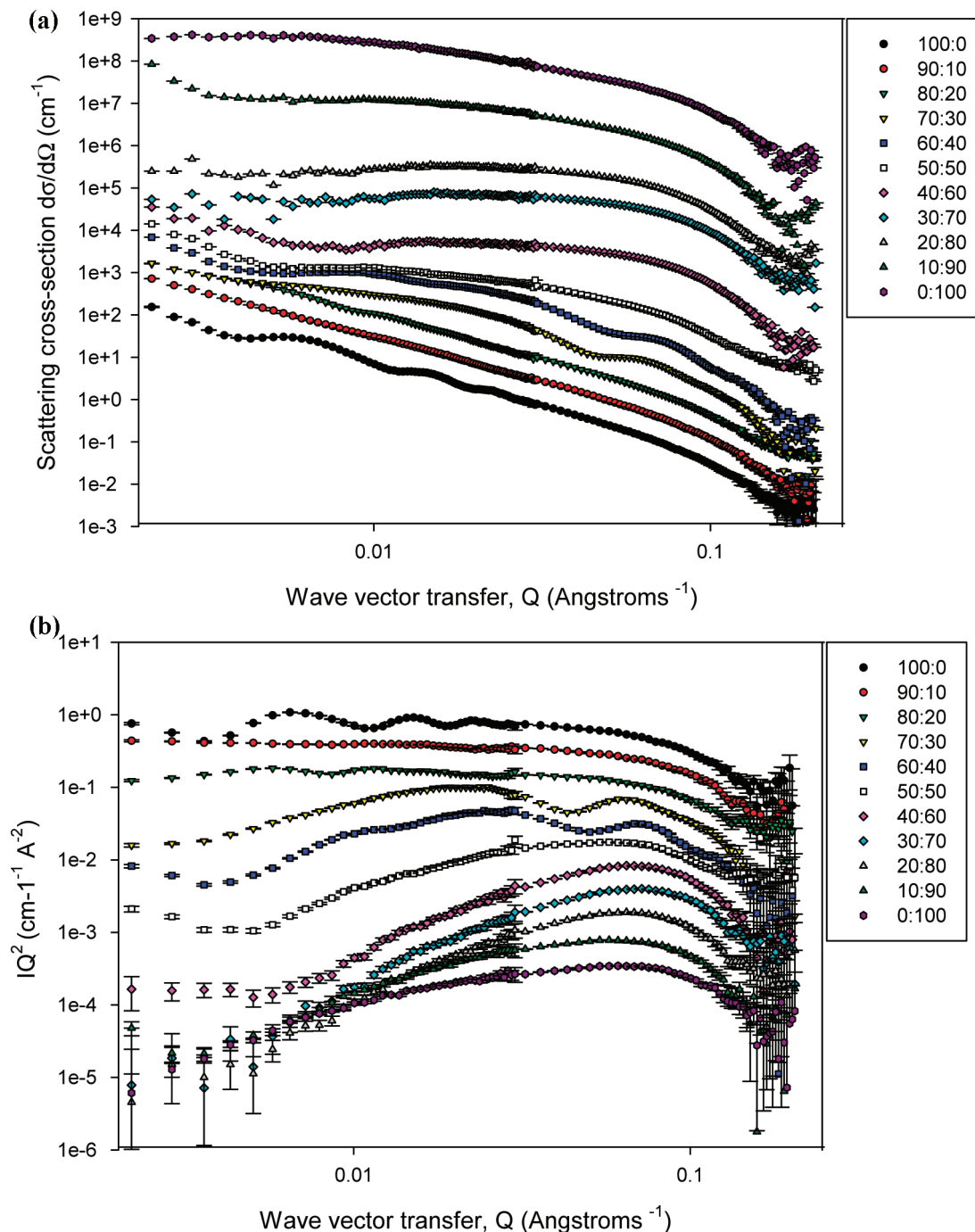
Figure 2. SANS scattering data for 1.5 mM DHDAB/$C_{12}E_6$/D_2O at mole ratios of 100:0, 90:10, 80:20, 70:30, 60:40, 50:50, 40:60, 30:70, 20:80, 10:90, and 100:0. Apart from the data for 100:0, the curves are shifted vertically for clarity, and the symbol definitions are included: plotted as (a) scattering cross section, $d\sigma/d\Omega$ (in cm^{-1}), vs wave vector transfer, Q (Å^{-1}), and (b) $Q^2I(Q)$ vs Q.

$C_{12}E_{12}$ in the composition range of 0:100−100:0, plotted as scattering cross section, $d\sigma/d\Omega$, versus Q and $Q^2I(Q)$ versus Q.

The data in the composition range of 0:100−40:60 are consistent with relatively small polydisperse globular micelles. Apart from the increase in micelle charge as the solutions become richer in DHDAB, there is little evidence of any significant systematic change in micelle size. That is, the scattering is relatively invariant with composition in that range of solution composition. The scattering from the solutions richer in DHDAB than 40:60 has a Q^{-2} dependence or a component of Q^{-2} scattering. In the composition range of 100:0−80:20, the scattering is purely Q^{-2} and is consistent with lamellar scattering. However, notably in comparison with the data for DHDAB/$C_{12}E_6$, the

oscillations in the data (in the region of $Q < 0.03$ Å^{-1}) are less visible (apart from the data for a composition of 100:0), and this is consistent with a more flexible membrane. At intermediate compositions (70:30−50:50), the scattering is consistent with the coexistence of planar and micellar components, and this is most clearly identified in the $Q^2I(Q)$ versu Q plots in Figure 6b. The scattering data in the purely lamellar and micellar regions have been analyzed quantitatively using the Nallet model[27] and the Hayter−Penfold core−shell model.[26] Typical models fits are shown in Figures 2 and 3 in the Supporting Information, and the key model parameters are summarized in Table 3.

From the detailed evaluation of the scattering data at 1.5 mM, it is evident that the mixed lamellar/micellar region is
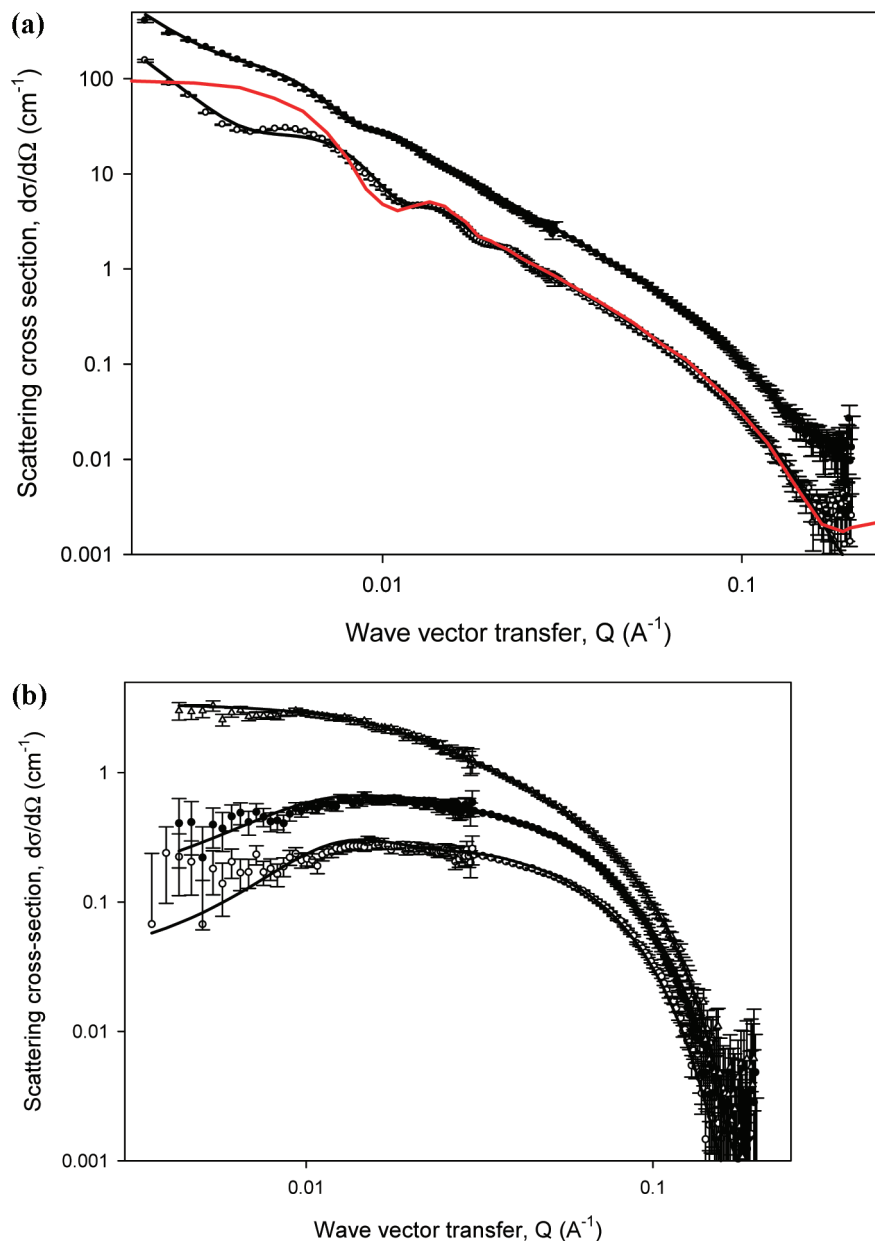
Figure 3. SANS scattering data, $d\sigma/d\Omega$ (in cm^{-1}) vs Q (Å^{-1}) for 1.5 mM DHDAB/C$_{12}$E$_6$/D$_2$O (a) for compositions 100:0 (o) and 80:20 (●) and (b) for compositions 30:70 (o), 20:80 (●), and 10:90 (Δ). The solid lines are model fits as described in the text and for the parameters summarized in Table 1. The different plots are offset vertically for clarity. Included in Figure 3a is a calculated curve (red) for the best fit for the core + shell model for DHDAB from ref 14.

Table 1. Key Model Parameters for 1.5 mM DHDAB/C$_{12}$E$_6$ from Quantitative Analysis

	100:0−80:20 Nallet Analysis			
solution composition (mole % DHDAB/C$_{12}$E$_6$)	layer spacing, d (Å) (±10)	layer thickness, δ (Å) (±0.2)	Caille parameter, η (±0.005)	number of layers, N (±1)
100:0	850	34.7	0.12	2
90:10	1150	36.0	0.11	2
80:20[a]	1140	36.2	0.10	2

	10:90−30:70 Micelle Analysis						
solution composition (mole % DHDAB/C$_{12}$E$_6$)	surfactant concentration (mM)	aggregation number, v	surface charge, z (±1)	inner radius, $R1$ (Å) (±0.5)	outer radius, $R2$ (Å) (±0.5)	ext (±0.05)	e (±0.1)
10:90	1.5	450 ± 20	1	17.2	22.6	1.0	7.9
20:80	1.5	190 ± 10	23	21.5	27.3	1.15	2.0
30:70	1.5	140 ± 10	25	20.9	25.9	1.20	1.8

[a] Low level of micellar scattering present.

extended to more cationic-rich compositions. The data indicate that there is some evidence of a micellar component even at

compositions as rich as 80:20 in DHDAB. The lamellar/planar structure is best described as bilamellar vesicles in which the

(a)

(b)
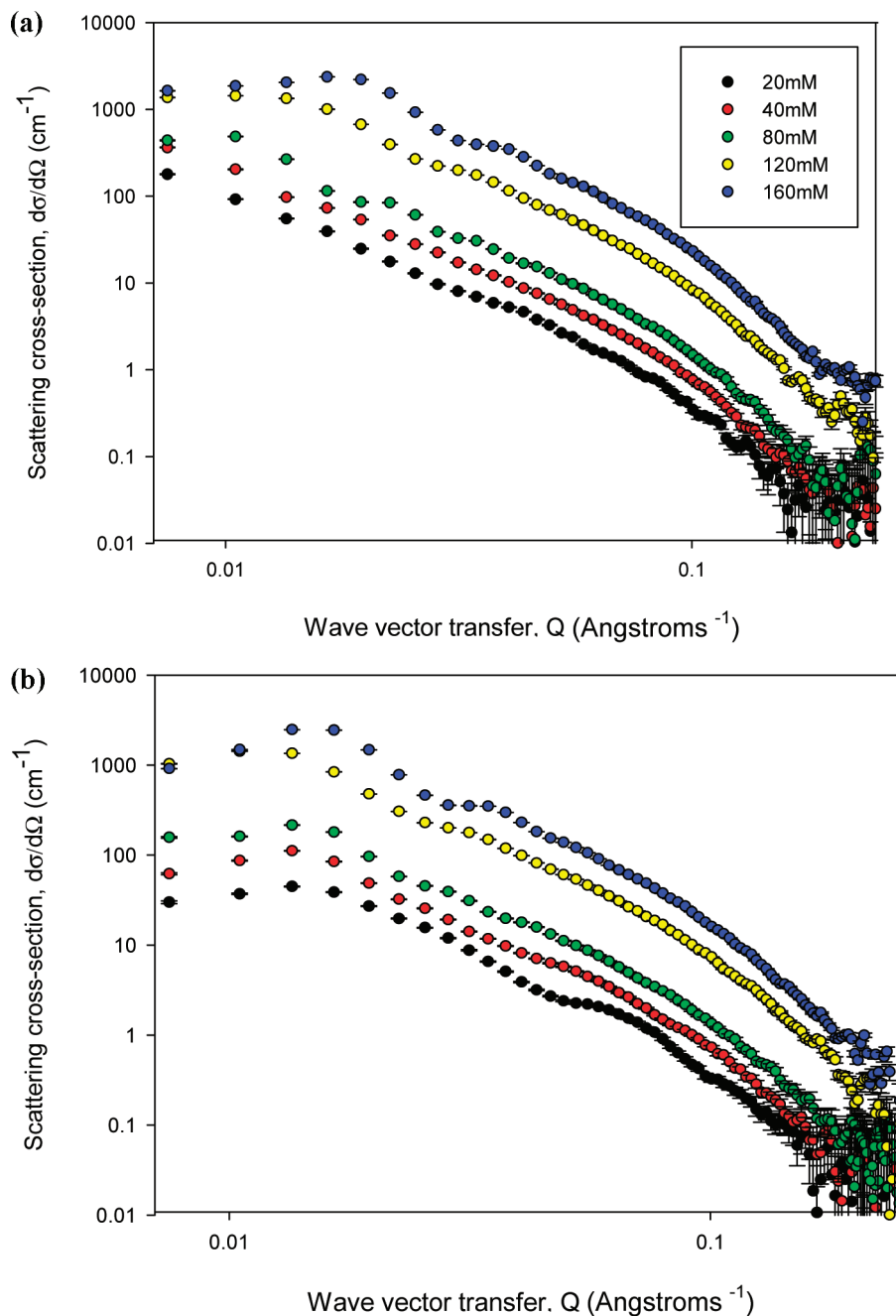
Figure 4. SANS scattering data, $d\sigma/d\Omega$ (in cm^{-1}) vs Q (Å^{-1}), for DHDAB/C$_{12}$E$_6$/D$_2$O (a) 80:20 at 20, 40, 80, 120, and 160 mM and (b) at 50:50. Symbol definition is included.

Table 2. Key Model Parameters for DHDAB/C$_{12}$E$_6$ Mixtures at Higher Surfactant Concentrations from Nallet Analysis

solution concentration and composition (mole % DHDAB/C$_{12}$E$_6$)	layer spacing, d (Å) (± 10)	layer thickness, δ (Å) (± 0.2)	Caille parameter, η (± 0.002)	number of layers, N
20 mM 80:20	890	31.8	0.013	5 ± 1
40 mM 80:20	680	33	0.003	35 ± 4
80 mM 80:20	540	31	0.02	5 ± 1
120 mM 80:20	360	31.3	0.2	3 ± 1
160 mM 80:20	320	31.6	0.1	6 ± 1
10 mM 65:35	730	34	0.011	38 ± 4
20 mM 65:35	730	34	0.006	22 ± 4
40 mM 65:35	650	33.7	0.005	34 ± 4
60 mM 65:35	590	32.1	0.01	25 ± 4

lamellar spacing increases as the cationic surfactant is diluted by the nonionic surfactant (as also observed for DHDAB/C$_{12}$E$_6$). However, there is a notable difference for the addition

of C$_{12}$E$_{12}$. As the amount of C$_{12}$E$_{12}$ increases, the Caille parameter increases significantly, and this is indicative of the membrane becoming more flexible. In contrast, the addition
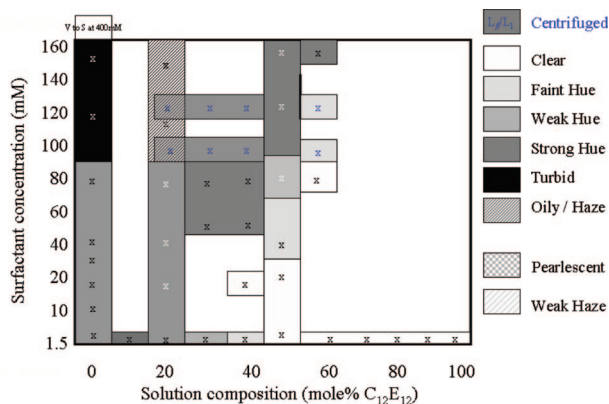
Figure 5. The same as for Figure 1, but for DHDAB/C$_{12}$E$_{12}$.

of C$_{12}$E$_6$ appears to have less of an impact upon membrane rigidity. In the purely micellar region (at 1.5 mM), the mixed DHDAB/C$_{12}$E$_{12}$ micelles are systematically smaller than those observed for DHDAB/C$_{12}$E$_6$, and grow only slightly with increasing DHDAB content. This is consistent with the significantly increased impact of C$_{12}$E$_{12}$ with its greater intrinsic curvature of aggregates associated with the larger E$_{12}$ headgroup.

At higher surfactant concentrations, the more extensive mixed micellar/lamellar coexistence is still evident in the data, but the variations in the microstructure, for 10−160 mM and in the composition range of 80:20−50:50, are less complicated. Here the scattering is consistent with L$_\beta$/L$_1$ coexistence (Figure 4 in the Supporting Information). The corresponding data for pure DHDAB is entirely blv. However, between pure DHDAB and 70:30 DHDAB/C$_{12}$E$_{12}$ (that is, at 80:20) the evolution of the structure is complex, as shown in Figure 4 in the Supporting Information. It evolves from blv/L$_1$ coexistence to mlv, to L$_\beta$, or to L$_\beta$/L$_1$ coexistence as the total surfactant concentration increases. DHDAB/C$_{12}$E$_{12}$ scattering data (plotted as $Q^2I(Q)$ vs Q) for surfactant concentrations of 5, 20, 80 mM and surfactant compositions of 80:20, 70:30, 60:40, and 50:50 are presented in Figure 4 in the Supporting Information. For compositions of 50:50, 60:40, and 70:30, the scattering at high Q (>0.02) is consistent with micellar scattering, whereas at low Q (<0.02) it is typical of the scattering from relatively rigid lamellar structures, with a characteristic slope of Q^{-2}. At a composition of 80:20, only the lamellar component is evident. At 5 mM, the Bragg oscillations from the lamellar structure are not particularly pronounced, indicating that the number of layers is small. (A detailed quantitative analysis of 80:20 indicates that this is 2, bilamellar.) As the surfactant concentration increases, the visibility of the Bragg oscillations increases significantly, consistent with a transition from blv to mlv or L$_\beta$ for compositions of 50:50, 60:40, and 70:30. The quantitative analysis at 80:20 indicates a transition from blv to mlv to L$_\beta$ in the concentration range of 5−40 mM. At a concentration of 80 mM (Figure 4c in the Supporting Information), the aggregation is in the form of L$_\beta$/L$_1$ (or mlv/L$_1$). Where a Nallet type analysis has been possible at higher surfactant concentrations, the key model parameters are summarized in Table 4.

iii. DHDAB/C$_{12}$E$_6$ (C$_{12}$E$_{12}$) Aggregate Compositions. At 1.5 mM, measurements were also made for the isotopic combinations of *h*-DHDAB/*h*-C$_{12}$E$_6$/D$_2$O and *d*-DHDAB/*h*-C$_{12}$E$_6$/D$_2$O. From the ratio of the scattering intensities extrapolated to zero Q, the aggregate composition can be estimated..[31] The data (shown in Figure 1a in the Supporting Information) show that, within experimental error, the aggregate composition reflects

the solution composition. Similar measurements over an extended Q range (5 × 10^{-5} to 2 × 10^{-3} Å^{-1}) using USANS[32] also confirm this evaluation.

Similar measurements were also made at 1.5 mM for DHDAB/C$_{12}$E$_{12}$ over the whole solution composition range with two different isotopically labeled combinations of DHDAB/C$_{12}$E$_{12}$. The results are summarized in Figure 1b in the Supporting Information and also indicate that within experimental error the aggregate composition is close to the solution composition. Because the measurements were made at a concentration much greater than the critical aggregation concentration, cac, it would be expected from regular solution theory and related thermodynamic treatments[2] that the aggregate compositions should reflect the solution composition, consistent with what is observed.

4. Discussion

I. Phase Behavior. From a combination of the optical texture observations and the interpretation of the scattering data, the phase behavior of the DHDAB/C$_{12}$E$_6$ and DHDAB/C$_{12}$E$_{12}$ mixtures has been deduced. The phase diagrams for both surfactant mixtures are shown (as surfactant concentration versus solution composition) in Figure 7a,b.

For both mixtures, the nonionic-rich regions are dominated by a micellar phase that extends to solution compositions richer in cationic surfactant for DHDAB/C$_{12}$E$_{12}$ than for DHDAB/C$_{12}$E$_6$. At intermediate compositions, the micellar phase coexists with a planar or lamellar phase (blv, mlv, or L$_\beta$), and this coexistence region is much more extensive (in both the range of compositions and concentrations) for DHDAB/C$_{12}$E$_{12}$. The cationic-rich region of the phase diagram is predominantly blv, mlv, or L$_\beta$.

The measurements were made at 30 °C, well below the L$_\beta$/L$_\alpha$ transition temperature The L$_\beta$/L$_\alpha$ transition temperature for pure DHDAB was measured by DSC[14] and is in the range of 42−44 °C. It is only slightly reduced in the presence of the cosurfactants used here. Henc,e it is reasonable to assume that the lamellar structures are L$_\beta$ and not L$_\alpha$. This is also supported by the bilayer thicknesses obtained from the quantitative analysis of the data, which implies significant interdigitation (δ is <2 L, where l is the fully extended alkyl chain length; l = 21.7 Å for a C$_{16}$ alkyl chain).

Broadly similar behavior has been reported by Penfold et al.[3] in other related dialkyl chain cationic/nonionic surfactant mixtures but was not quantified in such detail. Similar behavior has also been reported by Penfold et al.[33] for mixtures of sodium 6-dodecyl benzene-4 sulfonate/C$_{12}$E$_8$ mixtures in the presence of CaCl$_2$. Barraleiro et al.[34] and Feitosa et al.[35] have reported micelle-to-vesicle transitions in di-C$_{18}$DAB/C$_{12}$E$_8$ surfactant mixtures, and Alves et al.[36] and Kodama et al.[37] have reported similar data for di-C$_{18}$DAB/C$_{18}$TAB mixtures. Similar lamellar-to-micellar transitions have been observed in a range of phospholipids/surfactant mixtures.[4,38–40]

(31) Staples, E.; Penfold, J.; Thompson, L.; Tucker, I.; Hines, J. D.; Thomas, R. K.; Lu, J. R. *Langmuir* **1995**, *11*, 2479.

(32) Tucker, I.;. Penfold, J.;. Barker, J.;. Mildner, D. Unpublished results

(33) Penfold, J.; Thomas, R. K.; Dong, C. C.; Tucker, I.; Metcalfe, K.; Golding, S.; Grillo, I. *Langmuir* **2007**, *23*, 10140.

(34) Barreleiro, P. C. A.; Olfsson, G.; Brown, W.; Edwards, K.; Bonassi, N. M.; Feitosa, E. *Langmuir* **2002**, *18*, 1024.

(35) Feitosa, E.; Bonassi, N. M.; Loh, W. *Langmuir* **2006**, *22*, 4512.

(36) Alves, F. R.; Zaniquelli, M. E. D.; Loh, W.; Castanheira, E. M. S.; Real Oliveira, M. E. C. D.; Feitosa, E. *J. Colloid Interface Sci.* **2007**, *316*, 132.

(37) Kodama, T.; Ohta, A.; Toda, K.; Katada, T.; Asakawa, T.; Miyagishi, A. *Colloids Surf., A* **2006**, *277*, 20.

(38) LeMaire, M.; Champeil, P.; Mollerl, J. V. *Biochim. Biophys. Acta* **2000**, *1508*, 86.

(39) Heerklotz, H.; Seelig, J. *Biochim. Biophys. Acta* **2000**, *1508*, 69.

(40) Lichenberg, D.; Opatowski, E.; Kozlov, M. M. *Biochim. Biophys. Acta* **2000**, *1508*, 1.
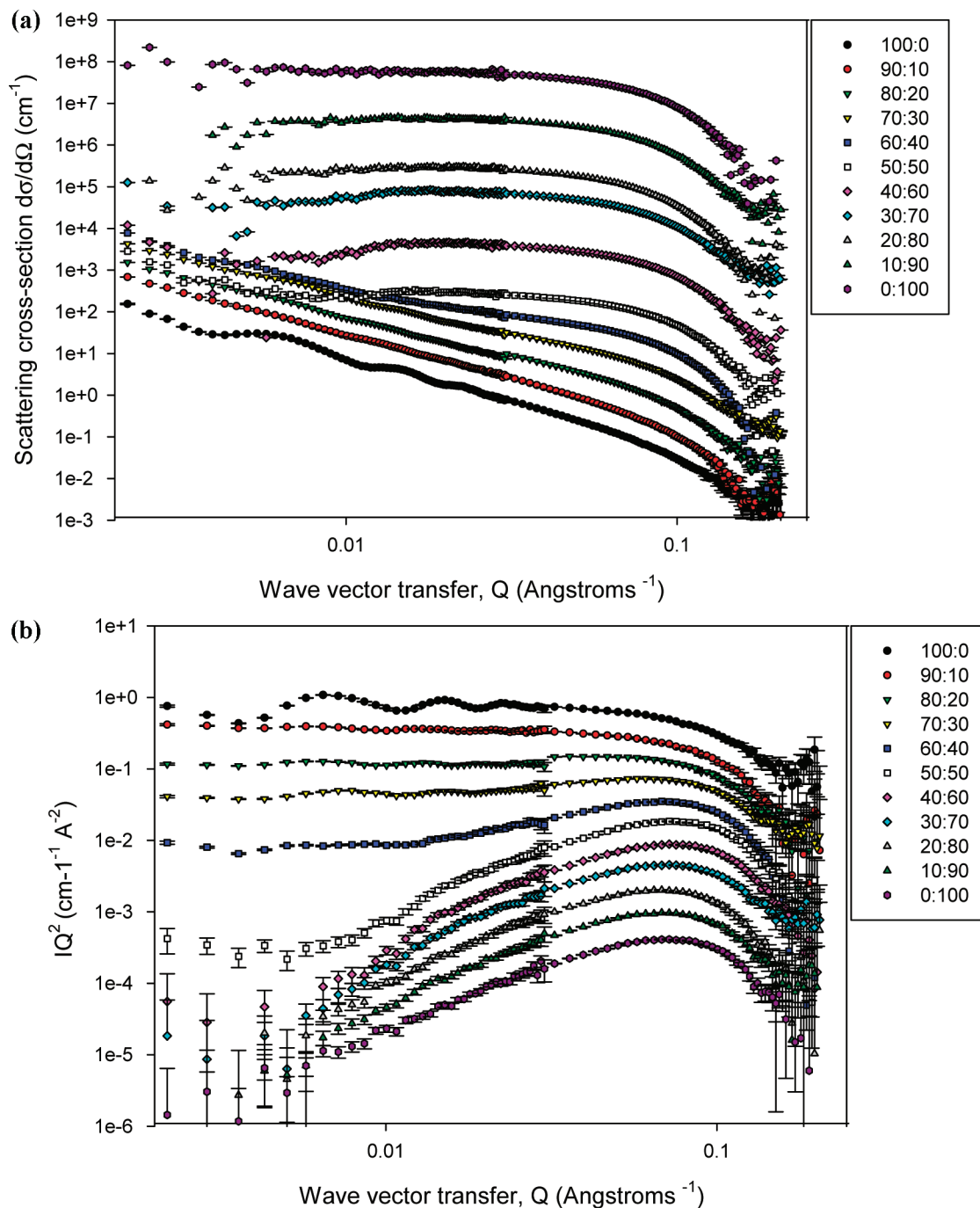
Figure 6. The same as for Figure 2, but for DHDAB/C$_{12}$E$_{12}$.

The nature of the mixed DHDAB/nonionic micelles in the nonionic-rich micellar region and the extent of that region reflect the relative curvatures of the aggregates associated with the two nonionic surfactants, C$_{12}$E$_6$ and C$_{12}$E$_{12}$. The smaller globular micelles for DHDAB/C$_{12}$E$_{12}$ compared to DHDAB/C$_{12}$E$_6$ (Tables 1 and 3) and the larger extent of the mixed-phase region for DHDAB/C$_{12}$E$_{12}$ are associated with the greater curvature of C$_{12}$E$_{12}$ aggregates compared to that of C$_{12}$E as a result of its bulkier headgroup.

From the Israelachvili, Ninham, and Mitchell packing considerations,[41] the aggregate packing parameter pp (where pp is defined as pp = V/Al, V is the volume/chain, A is the area/molecule, and l is the fully extended chain length; for pp < $^1/_3$ the aggregates are small globular micelles, for $^1/_3$ < pp < $^1/_2$ they are elongated micelles, and for pp > $^1/_2$ they are planar) for

C$_{12}$E$_6$ and C$_{12}$E$_{12}$ aggregates is 0.36 and 0.27, respectively, (assuming V = 330 Å^3, l = 16.7 Å, and A = 55 Å^2 for pure C$_{12}$E$_6$ and V = 330 Å^3, l = 16.7 Å, and A = 72 Å^2 for pure C$_{12}$E$_{12}$). Whereas pure C$_{12}$E$_{12}$ micelles are in the regime consistent with small globular micelles, C$_{12}$E$_6$ in contrast is just in the regime corresponding to growth or elongation. This is consistent with the observations for the micellar region of both DHDAB/nonionic mixtures. The pp for DHDAB is 0.68 (using V = 850 Å^3, l = 21.7 Å, and A = 60 Å^2 for pure DHDAB). Assuming ideal mixing, composition weighted values of V, A, and l from the pure components are used to calculate a mean or equivalent pp for the mixtures. The variation in the equivalent or mean pp with solution composition for both DHDAB/C$_{12}$E$_{12}$ and DHDAB/C$_{12}$E$_6$ is shown in Figure 8.

Table 3. Key Model Parameters for 1.5 mM DHDAB/C$_{12}$E$_{12}$ from Quantitative Analysis

		Nallet Analysis		
solution composition (mole % DHDAB/C$_{12}$E$_{12}$)	layer spacing, d (Å) ($\pm$10)	layer thickness, δ (Å) ($\pm$0.2)	Caille parameter, η ($\pm$0.002)	number of layers, N ($\pm$1)
100:0	850	34.7	0.07	2
90:10	1220	35.1	0.32	2
80:20[a]	1030	35.1	0.42	2
70:30[a]	860	35.1	0.26	2

			Micellar Analysis				
solution composition (mole % DHDAB/C$_{12}$E$_{12}$)	surfactant concentration (mM)	aggregation number, ν ($\pm$5)	surface charge, z ($\pm$1)	inner radius, $R1$ (Å) ($\pm$0.5)	outer radius, $R2$ (Å) ($\pm$0.5)	polydisperisity, σ ($\pm$0.02)	κ_{dh} (Å^{-1})
0:100	1.5	65	0.0	16.8	29.3	0.12	0.03
10:90	1.5	79	0.0	16.8	31.3	0.12	0.03
20:80	1.5	82	15	16.8	31.8	0.12	0.05
30:70	1.5	71	22	16.8	30.2	0.12	0.07
40:60	1.5	66	20	16.8	29.8	0.12	0.07

[a] A low level of micellar scattering is present.

Table 4. Key Model Parameters for DHDAB/C$_{12}$E$_{12}$ Mixtures at Higher Surfactant Concentrations from Nallet Analysis

surfactant concentration and composition (mole % DHDAB/C$_{12}$E$_{12}$)	layer spacing, d (Å) ($\pm$10)	layer thickness, δ (Å) ($\pm$0.2)	Caille parameter, η ($\pm$0.002)	number of layers, N
20 mM 80:20	600	32.9	0.002	70 $\pm$ 8
40 mM 80:20	550	34.7	0.01	54 $\pm$ 8
80 mM 80:20[a,b]	490	33.0	0.015	38 $\pm$ 6
120 mM 80:20[a]	390	33.5	0.035	20 $\pm$ 4
160 mM 80:20[a]	330	31.9	0.19	38 $\pm$ 6
50 mM 70:30	380	32.0	0.005	28 $\pm$ 4

[a] Relatively poor fits due to a small micellar contribution that is not included in the modeling. [b] Relatively poor fit due to a small micellar contribution and MLV/L$_\beta$ coexistence.

Although not in accurate quantitative agreement, the general trends and the differences in those trends for DHDAB/C$_{12}$E$_{12}$ and DHDAB/C$_{12}$E$_6$ are well predicted by the simple packing criteria. In particular, the differences between DHDAB/C$_{12}$E$_{12}$ and DHDAB/C$_{12}$E$_6$ can be rationalized in terms of the increased curvature associated with C$_{12}$E$_{12}$ aggregates compared to that for C$_{12}$E$_6$. A similar approach was used by Junquera et al.[42] to explain the transition from micelles to vesicles in a mixture of dialkyl chains and single-chain cationic surfactants: di-C$_{12}$DAB and DTAB; di-C$_{12}$DAB/nonionic surfactant mixtures.[43] Vesicle formation does not always occur, and Lusvardi et al.[44] have discussed the changes in packing arising in the mixed micelles of DDAB/DTAB surfactant mixtures. In catanionic surfactant mixtures, for example, SDS/DDAB in refs 44 and 46, the interplay between electrostatic and packing effects results in the formation of vesicle structures.

Although it is difficult to quantify the structures in the mixed-phase regions, it is relatively straightforward to identify the coexistence of lamellar and micellar structures. Furthermore, it is evident that as the solution becomes richer in the cationic surfactant in the mixed-phase region the balance of components shifts from L$_1$/L$_\beta$ to L$_\beta$/L$_1$. For both mixtures at intermediate compositions and concentrations, there is also evidence of L$_\beta$/mlv coexistence. At higher surfactant concentrations ($>$ 10 mM) for pure DHDAB, the phase behavior is consistent with mixed blv phases.[14] A key feature of the phase behavior of the DHDAB/C$_{12}$E$_6$ and DHDAB/C$_{12}$E$_{12}$ mixtures is the variation in the form of the planar structures that are observed for cationic-rich compositions. Although the scattering for the cationic-rich compositions has a Q^{-2} dependence indicative of planar structures such as lamellar fragments or vesicles, it has been demonstrated that quite a rich variation in the detailed morphology exists. At 1.5 mM for both the DHDAB/nonionic mixtures and for pure DHDAB to higher surfactant concentrations the predominant

form of the planar structures is that of bilamellar vesicles. Similar structures are also observed for DHDAB/C$_{12}$E$_3$ mixtures, and a more detailed discussion of the determination and quantification of those structures for DHDAB and DHDAB/C$_{12}$E$_3$ is presented elsewhere.[14,15]

However, some further discussion in the context of the data presented here is justified to rationalize the deduced phase behavior. For the scattering data in this region, there are relatively weak but clearly visible and well-defined oscillations in the Q^{-2} dependence of the scattering. An initial inspection would suggest that this arises from oscillations in the form factor associated with the overall size of relatively monodisperse unilamellar to multilamellar vesicles. Such analyses have been extensively reported for many other vesicle-forming systems, such as phospholipids and phospholipids/cosurfactant mixtures.[47] For the data presented here, the periodicity of the oscillations is not consistent with the form factor for a core + shell model of the scattering, as previously demonstrated and discussed in detail for DHDAB alone.[14] The inadequacy of this model to reproduce the data is illustrated here in Figure 3a. However, the periodicity is consistent with a relatively large lamellar or multilamellar repeat distance, and the Nallet description of lamellar scattering[27] provides a good quantitative description of the data; see Figure 3 and the parameters in Tables 1–4.

(41) Israelachvili, J. N.; Mitchell, D. J.; Ninham, B. W. *J Chem. Soc, Faraday Trans 2* **1976**, *72*, 1525.

(42) Junquera, E.; Arranz, R.; Aicart, E. *Langmuir* **2004**, *20*, 6619.

(43) Junquera, E.; deBurgo, P.; Arranz, R.; Llorca, O.; Aicart, E. *Langmuir* **2005**, *21*, 1795.

(44) Lusvardi, K. M.; Full, A. P.; Kaler, E. W. *Langmuir* **1995**, *11*, 487.

(45) Marques, E. F.; Regev, O.; Khan, A.; da Gracia Migel, M.; Lindman, B. *J. Phys. Chem. B* **1999**, *103*, 8353.

(46) Marques, E. F.; Regev, O.; Khan, A.; da Gracia Migel, M.; Lindman, B. *J. Phys. Chem. B* **1998**, *102*, 6746.

(47) Katsaras, J. *Curr. Opin. Colloid Interface Sci.* **2007**, *12*, 17.

(a)

(b)
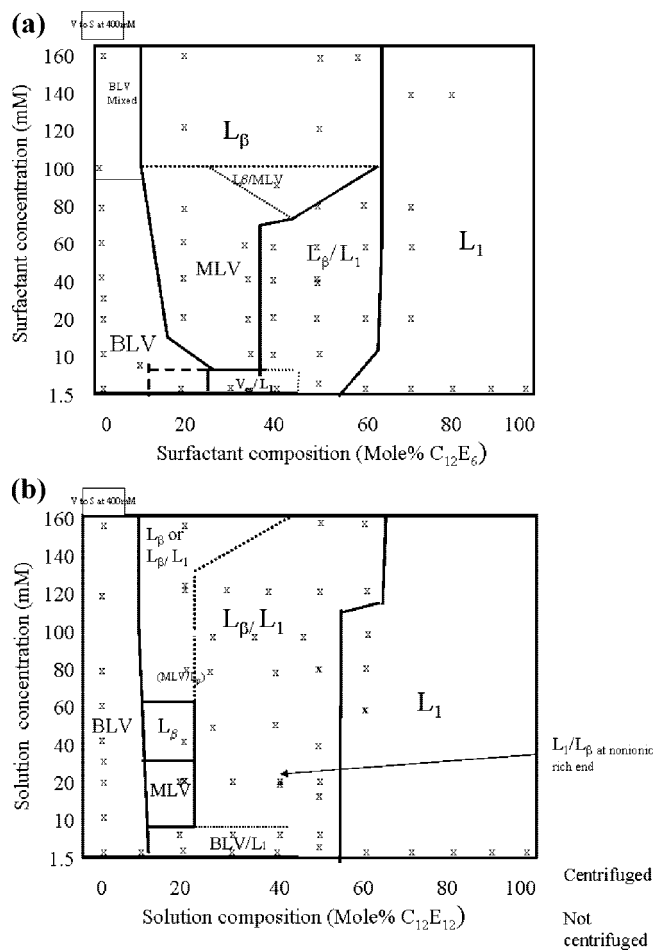
Figure 7. Phase diagram, plotted as surfactant concentration vs surfactant composition, delineating the different structural regions at 30 °C for DHDAB/C$_{12}$E$_6$ (a) and DHDAB/C$_{12}$E$_{12}$ (b) (where each x denotes the position where a measurement was made).
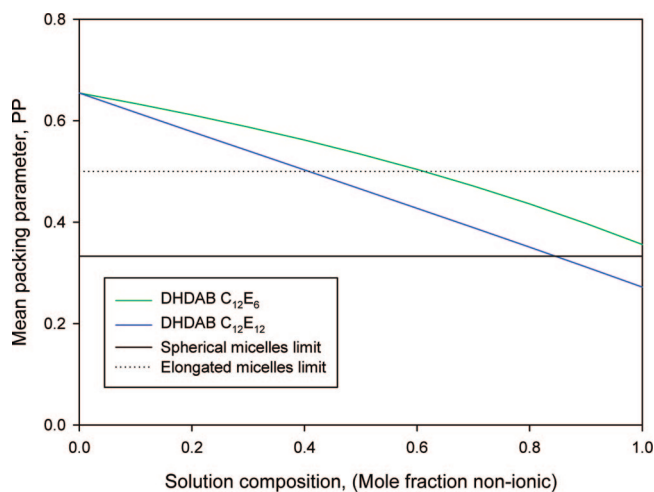
Figure 8. Variation in packing parameter, pp, with solution composition for DHDAB/C$_{12}$E$_6$ (green line) and DHDAB/C$_{12}$E$_{12}$ (blue line). The horizontal lines (- - -) denote the transitions from globular micelles to elongated structures and from elongated to planar aggregates.

This interpretation is also reinforced by cryo-TEM images for pure DHDAB, which clearly show the presence of vesicles,[14] and these data have also been reproduced in Figure 5 in the Supporting Information. Furthermore, light scattering (PCS) and USANS measurements have provided an estimate of the overall size of the lamellar aggregates and of their polydispersity. For

Table 5. Variation in Particle Size and Particle Size Distribution for 1.5 mM DHDAB/C$_{12}$E$_{12}$ at 30 °C from PCS Analysis

solution composition (mole % DHDAB/C$_{12}$E$_{12}$)	mean diameter (Å) (±80 Å unless stated otherwise)	polydispersity, σ (±0.05)
100:0	2280	0.60
80:20	3300	0.40
70:30	2600	0.55
60:40	1780	0.14
50:50	1300	0.65
40:60	320 ± 40	0.20
30:70	260 ± 30	0.15

Table 6. Variation in Particle Size and Size Distribution for DHDAB/C$_{12}$E$_6$ at 30 °C from USANS Analysis

solution concentration and composition (mole % DHDAB/C$_{12}$E$_6$)	mean diameter (Å) (±100)	polydispersity, σ (±0.05)
1.5 mM 100:0	2750	0.5
80 mM 50:50	17 660	0.62

DHDAB,[14] DHDAB/C$_{12}$E$_{12}$, and DHDAB/C$_{12}$E$_6$, the light scattering at 1.5 mM is interpreted in terms of relatively large vesicles with a large polydispersity. For DHDAB,[14] complementary light scattering (PCS) and USANS data are consistent with a mean particle radius of ~0.1−0.2 μm (also consistent with the parameters inferred from the Nallet analysis) and a polydispersity of ~40−50%. The corresponding PCS measurements for 1.5 mM DHDAB/C$_{12}$E$_{12}$ at different solution compositions are listed in Table 5. In Table 6, the corresponding parameters obtained from the analysis of the USANS data for 1.5 mM DHDAB and 80 mM DHDAB/C$_{12}$E$_6$ are listed, and the corresponding USANS data and model fits are shown in Figure 6 in the Supporting Information.

The USANS model parameters for 1.5 mM DHDAB are consistent with that expected for a blv structure of the dimensions described. (See a more detailed discussion in ref 14). In contrast, the scattering for 80 mM 50:50 DHDAB/C$_{12}$E$_6$ is shifted to even lower Q, consistent with a larger scattering object. These data have been analyzed in terms of a globular particle, with a mean size of ~2 μm and a relatively large polydispersity. This is interpreted as arising from the lamellar fragments that exist in this region of the phase diagram. This interpretation of the data is consistent with the broader observations at the higher surfactant concentrations.

The size measurements from PCS and USANS and their consistency with the size inferred from the Nallet analysis strongly support the interpretation in terms of the blv/mlv structures at lower surfactant concentrations and a transition to lamellar fragments, L$_\beta$, at higher surfactant concentrations. Furthermore, the large degree of polydispersity obtained from PCS and USANS would completely smear out any oscillations in the core + shell interpretation of the scattering, contrary to what is observed here. The occurrence of such bilamellar and multilamellar vesicle structures with relatively large lamellar spacings observed here in dilute solution has been reported in other vesicle-forming systems. Clear evidence from predominantly cryo-TEM images have been presented by Gonzales et al.[48] for SDBS/imidozoline mixtures, by Feitosa et al.[49] for di-C$_{18}$DAB, and by McGillivray et al.[50] for di-C$_{12}$DAB.

(48) Gonzales, Y. L.; Stjerndahl, M.; Danino, D.; Kaler, E. W. *Langmuir* **2004**, *20*, 7053.
(49) Feitosa, E.; Barreleiro, P. C. A. *Prog. Colloid Polym. Sci.* **2004**, *128*, 163.
(50) McGillivray, D.; Thomas, R. K.; Rennie, A. R.; Penfold, J.; Sivia, D. S. *Langmuir* **2003**, *19*, 7719.

ii. Membrane Rigidity. From the Nallet analysis of the lamellar regions of the phase diagram and from some limited areas of the lamellar/micellar coexistence region, the Caille parameter (along with the number of layers and the bilayer and lamellar thicknesses) is obtained. The Caille parameter, η, is inversely related to the rigidity of the membrane through

$$\eta = \frac{Q_0^2 k_B T}{8\pi\sqrt{KB}} \tag{9}$$

where $K = \kappa/d$ and $Q_0 = 2\pi/d$. B is the bilayer compressibility, and K is the bending modulus. We can also directly express it in terms of the product kB such that

$$\kappa B = \left(\frac{\pi k_B T}{2d^{\frac{3}{2}}\eta}\right)^2 \tag{10}$$

The values of κB obtained for DHDAB/$C_{12}E_6$ and DHDAB/$C_{12}E_{12}$ are summarized in Tables 7 and 8.

From this analysis, we can quantify the variation in membrane properties (rigidity) with composition and concentration from the η and κB values.

At low surfactant concentrations (1.5 mM) for both DHDAB/$C_{12}E_{12}$ and DHDAB/$C_{12}E_6$, the Caille parameter is relatively small, typically ≤ 0.1, and this implies a relatively stiff or rigid membrane. This is similar to values reported elsewhere for charge stabilized membranes. For example, typical values for AOT and DDAB are $\sim 0.15-0.25$[27] and $\sim 0.02-0.08$ for other related dichain cationic/nonionic mixtures.[3] In contrast, for the lamellar phase of $C_{12}E_5$, which is stabilized by fluctuations,[51,52] the corresponding Caille parameter is in the range of $0.3-1.5$. For the DHDAB/$C_{12}E_6$ mixture, there is a 5-fold reduction in the Caille parameter with composition at low surfactant concentrations (over the limited composition and concentration range where it could be reliably extracted from the data without interference from the micellar component). An extensive evaluation of the change in membrane rigidity with surfactant concentration and composition is not possible for the DHDAB/$C_{12}E_{12}$ mixture because the impact of $C_{12}E_{12}$ is to promote the formation of mixed micelles more readily than $C_{12}E_6$. Hence, the occurrence of lamellar/micellar coexistence starting at more cationic-rich compositions hinders the Nallet-type quantitative analysis over a wide range of compositions and concentrations. However, at 1.5 mM it is evident that the addition of $C_{12}E_{12}$ to DHDAB has a much greater impact than $C_{12}E_6$. Notably, it results in a significant and immediate increase in the membrane flexibility or fluidity (a decrease in the rigidity). For DHDAB/$C_{12}E_6$, it has been possible to evaluate the impact of $C_{12}E_6$ on the membrane rigidity over a wider range of compositions and concentrations, especially to higher surfactant concentrations. This is consistent with the observations from previous studies, where the addition of a nonionic cosurfactant would be expected to fluidize membranes. Safinya et al.[53,] have demonstrated how the addition of an alkyl alcohol cosurfactants reduces membrane rigidity to the point where the membrane becomes stabilized by undulation forces rather than charge. Although $C_{12}E_{12}$ has a significant impact upon membrane rigidity, $C_{12}E_6$ in contrast does not fluidize the membranes to the same extent. This is attributed to the greater steric contribution of the E_{12} headgroup compared to that of the E_6 headgroup and the greater curvature associated with $C_{12}E_{12}$ aggregates and the greater ability to disrupt the membrane.

Although to some degree the changes in the Caille parameter, η, reflect changes in the membrane rigidity, the value of η has a strong dependence on d (the bilayer spacing, eq 9). However,

Table 7. Variation in Membrane Rigidity Product (κB) for DHDAB/$C_{12}E_6$ Mixtures at 30 °C

concentration and composition (mole % DHDAB/$C_{12}E_6$)	rigidity (κB) $\times$ 10^{-9} (ergs² cm⁻³)
1.5 mM 100:0	1.43 ± 0.02
1.5 mM 90:10	0.23 ± 0.01
1.5 mM 80:20	0.31 ± 0.01
20 mM 80:20	36 ± 5
40 mM 80:20	1550 ± 50
80 mM 80:20	69 ± 5
120 mM 80:20	2.3 ± 0.02
160 mM 80:20	13.8 ± 0.2
10 mM 65:35	90 ± 5
20 mM 65:35	310 ± 10
40 mM 65:35	635 ± 50
60 mM 65:35	2110 ± 50
94 mM 60:40	81 ± 10
80 mM 50:50	11.0 ± 0.02
120 mM 50:50	1.40 ± 02
160 mM 50:50	3.00 ± 02
160 mM 40:60	3.0 ± 0.02

Table 8. Variation in Membrane Rigidity Product (κB) with Solution Composition for DHDAB/$C_{12}E_{12}$ Mixtures

solution concentration and composition (mole % DHDAB/$C_{12}E_{12}$)	rigidity (κB) $\times$ 10^{-9} (ergs² cm⁻³)
1.5 mM 100:0	1.43 ± 0.02
1.5 mM 90:10	0.02 ± 0.01
1.5 mM 80:20	0.02 ± 0.01
1.5 mM 70:30	0.1 ± 0.01

recasting eq 9 in terms of the rigidity product κB provides a more direct indication of the variation in the membrane properties (rigidity) with surfactant concentration and composition. This is illustrated in Tables 7 and 8 where the changes in κB for the DHDAB/$C_{12}E_6$ and DHDAB/$C_{12}E_{12}$ mixtures are tabulated. At low surfactant concentration (1.5 mM), the greater impact of $C_{12}E_{12}$ over that of $C_{12}E_6$ on the membrane rigidity is clearly demonstrated in the variations in the κB product. The change in κB with the addition of $C_{12}E_{12}$ is ~ 10 times larger than for the addition of $C_{12}E_6$. For the DHDAB/$C_{12}E_6$ mixture, we have mapped the variations in κB (where evaluated) onto the corresponding phase diagram, and this is shown in Figure 9.

Given that from eq 10 κB depends upon d^3 and η^2, quite large variations in κB from relatively modest changes in d and η can arise, and this is especially illustrated by the variations listed in Table 7. The variations in κB with surfactant concentration and composition show a complex pattern. At low surfactant concentration (1.5 mM), the addition of the cosurfactant results in a decrease in κB, as discussed earlier for DHDAB/$C_{12}E_6$ and DHDAB/$C_{12}E_{12}$. For DHDAB/$C_{12}E_6$, the transition from blv to mlv at a surfactant concentration of ≥ 10 mM is accompanied by an increase in the membrane rigidity. However, at a composition of 80:20 the transition from mlv to L_β or L_β/L_1 observed at higher concentrations (80–100 mM) is accompanied by a decrease in the membrane rigidity. κB goes through a maximum around a concentration of 40 mM. Conversely, at a composition of 65:35, κB increases with increasing concentration (from 10 to 60 mm). The variations in κB at a composition of 50:50 are less significant. At the higher surfactant concentrations, there are other contributing factors, and a detailed interpretation of the data in Figure 9 and Tables 7 and 8 is not very
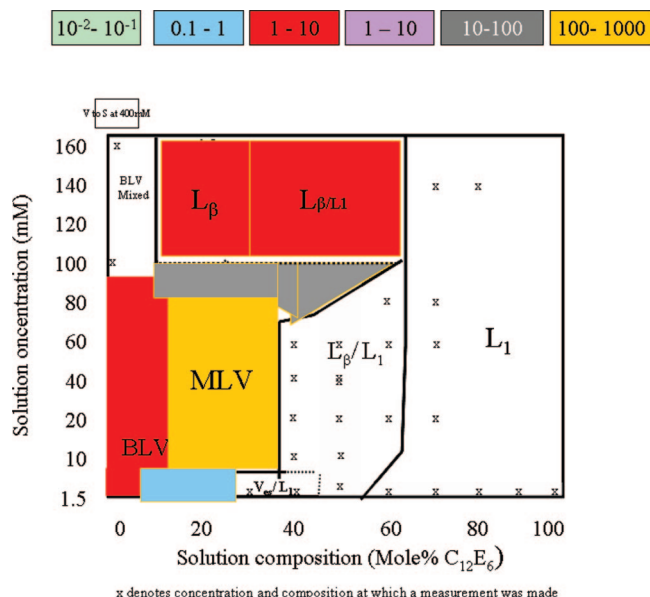
Figure 9. Variation in κB for DHDAB/$C_{12}E_6$ mapped onto the phase diagram from Figure 7a.

straightforward. For example, as discussed for DHDAB,[14] a variation in both κ and B could reasonably be expected as a result of both concentration and changes in counterion binding. Furthermore, in the mixed-phase region that was evaluated quantitatively (Figure 9), changes in osmotic pressure due to the coexisting micellar component are likely, and this has been observed to give rise to depletion effects in related systems.[3] Such effects could well explain the differences between the trends at compositions of 80:20 and 65:35.

Separation of the compressibility and bending modulii have been made by performing systematic studies on continuously swelling system[49,59] using the excess area method. However, the inability to use that approach for DHDAB has been discussed,[14] and the same arguments apply here. However, if we assume that the lamellar spacing and bilayer thickness are not changing dramatically within the range of the measurements, then it could be assumed that B is approximately constant and that changes in κB reflect changes in the membrane rigidity. To that end, we have considered the approach of Bryshke et al.,[53] who have discussed the relative stability of lamellar fragments and vesicles, in terms of the competition between the vesicle curvature energy and the disk (lamellar fragment) edge energy. This approach was applied to recent data for DHDAB.[14] Typical values of line tension and membrane rigidity are consistent with the formation of vesicles at low surfactant concentrations and apply equally to the DHDAB/$C_{12}E_6$ and DHDAB/$C_{12}E_{12}$ mixtures at low concentrations. Alternatively, Jung et al.[56] have considered the origins of the stability of spontaneously formed vesicles by comparing the contributions from undulations and spontaneous curvature. When the bending modulus, κ, is $\sim k_B T$, equilibrium unilamellar vesicles are stabilized by undulation forces, whereas for $\kappa \gg k_B T$ unilamellar vesicles are stabilized by the spontaneous curvature

(51) Diat, O.; Roux, D.; Nallet, F. *J. Phys. II* **1993**, *3*, 1427.
(52) Yang, B. S.; Lal, J.; Richetti, P.; Marques, C. M.; Russell, W. B.; Prud'homme, R. K. *Langmuir* **2001**, *17*, 5834.
(53) Safinya, C. R.; Sirota, E. B.; Roux, D.; Smith, G. S. *Phys. Rev. Lett.* **1989**, *62*, 1134.
(54) Safinya, C. R.; Roux, D.; Smith, G. S.; Sinha, S. K.; Dimon, P.; Bellocq, A. M. *Phys. Rev. Lett.* **1986**, *57*, 2718.
(55) Bryshke, K.; Bulut, S.; Olsson, U. *J. Phys. Chem. B* **2005**, *109*, 9265.
(56) Jung, H. T.; Codern, B.; Zasadsinski, J. A.; Lampieto, D. J.; Kaler, E. W. *Proc. Natl. Acad. Sci. U.S.A.* **2001**, *98*, 1853.

Figure 10. Phase diagrams for DHDAB/$C_{12}E_6$ and DHDAB/$C_{12}E_{12}$ plotted as nonionic vs cationic surfactant concentrations, where the lines labeled C_{sol} represents the L_1 boundary and C_{sat} represents the lamellar boundary.

and a narrow distribution of vesicle radii are favored and manipulation of the curvature can result in bilamellar vesicles. The polydispersity values obtained here (Tables 5 and 6) are broadly similar to those reported by Jung et al.[56]

For DHDAB,[14] we have calculated values of κ and B and their variation with surfactant concentration from expressions for κ and B for electrostatically stabilized membranes.[57,58] The variation with surfactant concentration is not at all predicted, although it is in broad quantitative agreement. In light of this and the additional complexity associated with the mixtures, we have not pursued this approach further.

iii. Membrane Solubilization. An analogy with membrane solubilization studies[38–40] provides further insight into the DHDAB/nonionic phase behavior and the differences in the impact of the two nonionic surfactants, $C_{12}E_6$ and $C_{12}E_{12}$. Hence in Figure 10 the major phase boundaries (L_1 to L_1/L_β, L_1/L_β to vesicle, L_v) from Figure 7a,b are reploted in terms of the nonionic and cationic surfactant concentrations.

In the plot, the upper boundary (labeled C_{sol}) can be considered to be a solubilization maximum. That is, it represents the maximum amount of DHDAB that can be solubilized or comicellized with the initially nonionic micelles before the formation of planar aggregates is more energetically favorable. Conversely, the lower boundary (labeled C_{sat}) can be considered to be the saturation concentration of nonionic surfactant in the initially cationic-rich membrane before the membrane structure is sufficiently disrupted that mixed micelle formation is favored. From Figure 10, it is evident that the greater curvature of $C_{12}E_{12}$ aggregates compared to that of $C_{12}E_6$ ensures that more cationic surfactant is comicellized before planar structures are formed. Conversely for the cationic-rich region, less $C_{12}E_{12}$ can be solubilized into the membrane before it is disrupted to an extent that micelle formation is more favorable.

5. Summary

The phase behavior of mixtures of the dialkyl chain cationic surfactant, DHDAB, and the nonionic surfactants, $C_{12}E_6$ and $C_{12}E_{12}$, has been quantified by SANS and other complementary experimental techniques. The evolution from planar structures (blv, mlv, and L_β) for cationic-rich compositions to relatively small globular micelles for nonionic-rich compositions is demonstrated. At intermediate compositions, the extent of the

mixed planar/micellar region has been quantified for both mixtures. The impact of the different preferred curvatures associated with the aggregates of the two nonionic surfactants on the phase behavior and on the rigidity of the lamellar structures has been demonstrated and, where possible, correlated.

Supporting Information Available: Variation in aggregate composition with solution composition for 1.5 mM DHDAB/$C_{12}E_6$ and 1.5 mM DHDAB/$C_{12}E_{12}$. SANS scattering data for DHDAB/$C_{12}E_{12}$. Replica cryo-TEM images of DHDAB in water. USCANS scattering data for DHDAB and DHDAB/$C_{12}E_6$. This material is available free of charge via the Internet at http://pubs.acs.org.

LA703702P

(57) Mitchell, D. J.; Ninham, B. W. *Langmuir* **2000**, *16*, 296.
(58) Roux, D.; Safinya, C. R. *J. Phys. (Paris)* **1988**, *49*, 30.
(59) Feyssingeas, E.; Martin, A.; Roux, D. *Europhys. J. E* **2005**, *18*, 219.